

# Energy based diffusion generator for efficient sampling of Boltzmann distributions

Yan Wang<sup>a</sup>, Ling Guo<sup>b</sup>, Hao Wu<sup>\*c</sup>, Tao Zhou<sup>d</sup>

<sup>a</sup>*School of Mathematical Sciences, Tongji University, Shanghai, China*

<sup>b</sup>*Department of Mathematics, Shanghai Normal University, Shanghai, China*

<sup>c</sup>*School of Mathematical Sciences, Institute of Natural Sciences and MOE-LSC, Shanghai Jiao Tong University, Shanghai, China, \*hwu81@sjtu.edu.cn,*

<sup>d</sup>*LSEC, Institute of Computational Mathematics and Scientific/Engineering Computing, AMSS, Chinese Academy of Sciences, Beijing, China*

---

## Abstract

Sampling from Boltzmann distributions, particularly those tied to high-dimensional and complex energy functions, poses a significant challenge in many fields. In this work, we present the Energy-Based Diffusion Generator (EDG), a novel approach that integrates ideas from variational autoencoders and diffusion models. EDG leverages a decoder to transform latent variables from a simple distribution into samples approximating the target Boltzmann distribution, while the diffusion-based encoder provides an accurate estimate of the Kullback-Leibler divergence during training. Notably, EDG is simulation-free, eliminating the need to solve ordinary or stochastic differential equations during training. Furthermore, by removing constraints such as bijectivity in the decoder, EDG allows for flexible network design. Through empirical evaluation, we demonstrate the superior performance of EDG across a variety of complex distribution tasks, outperforming existing methods.

*Keywords:* Boltzmann distribution, Energy-based model, Generative model, Diffusion model, Variational autoencoder

---

## 1. Introduction

In various fields such as computational chemistry, statistical physics, and machine learning, the challenge of sampling from a Boltzmann distribution corresponding to a high-dimensional and complex energy function is ubiquitous [1, 2]. Unlike training tasks for data-driven generative models, where

pre-sampled data can be utilized to learn complex distributions, sampling from Boltzmann distributions presents a unique and significant challenge due to the lack of readily available data [3, 4]. For example, simulating the phase transition of the Ising model can be framed as a sampling problem given the energy function, which presents a complex and difficult problem that has yet not to be effectively addressed [5, 6].

Markov Chain Monte Carlo (MCMC) methods [7], along with Brownian and Hamiltonian dynamics [8–11], have offered a pivotal solution to the challenge of sampling from high-dimensional distributions. These methods operate by iteratively generating candidates and updating samples, ultimately achieving asymptotic unbiasedness at the limit of infinite sampling steps. In recent years, researchers have proposed adaptive MCMC as a strategy for generating candidate samples, showcasing notable advancements in augmenting the efficiency and effectiveness of the sampling process [12–14]. However, the prolonged mixing time of MCMC still constrains its performance. Several studies have shown that using neural networks to construct and optimize proposal distributions in MCMC can significantly improve its efficiency [13, 15, 16]. However, there is still a lack of an effective and widely adaptable loss function to facilitate this optimization.

Variational inference (VI) is another crucial approach for addressing intractable distributions. VI leverages a generator capable of swiftly producing samples to approximate the target Boltzmann distribution, and the optimization of the generator’s parameters is then undertaken to minimize a statistical distance, such as the Kullback-Leibler (KL) divergence, between the distribution of the generated samples and the target distribution. Due to its ability to model complex distributions and provide explicit probability density functions, normalizing flow (NF) has been extensively applied to construct generators for VI methods [17–26]. However, the bijective nature of NFs imposes a constraint on their effective capacity, often rendering it insufficient for certain sampling tasks. Given the target density function and the generated samples, Stein Discrepancy [27, 28] provides a different means to evaluate the goodness of fit, while the computation of kernel functions and their gradients limits its performance in high-dimensional tasks. In addition, the combination of MCMC and VI methods stands as a current focal point in research [29–34]. This combination seeks to harness the strengths of both approaches, offering a promising avenue for addressing the challenges associated with sampling from high-dimensional distributions and enhancing the efficiency of probabilistic modeling.

With the prosperity of diffusion based generative models [35–38], they have been applied to address challenges in the sampling problem. By training time-dependent score matching neural networks, methods proposed in [39–41] shape the Gaussian distribution into complex target densities, employing the KL divergence as the loss function. To mitigate mode-seeking issues, [42] introduces the log-variance loss, showcasing favorable properties. Additionally, an alternative training objective is outlined in [43], relying on flexible interpolations of the energy function and demonstrating substantial improvements for multi-modal targets. However, a common drawback of these methods is their reliance on numerical differential equation solvers for computing time integrals, which can lead to substantial computational costs.

In this research endeavor, we present a novel approach termed the energy based diffusion generator (EDG), drawing inspiration from both the variational autoencoder (VAE) technique [44] and the diffusion model. The architecture of EDG closely resembles that of VAE, comprising a decoder and an encoder. The decoder is flexible in mapping latent variables distributed according to tractable distributions to samples, without the imposition of constraints such as bijectivity, and we design in this work a decoder based on generalized Hamiltonian dynamics to enhance sampling efficiency. The encoder utilizes a diffusion process, enabling the application of score matching techniques for precise and efficient modeling of the conditional distribution of latent variables given samples. Unlike existing diffusion-based methods, the loss function of EDG facilitates the convenient computation of unbiased estimates in a random mini-batch manner, removing the need for numerical solutions to ordinary differential equations (ODEs) or stochastic differential equations (SDEs) during training. Numerical experiments conclusively demonstrate the effectiveness of EDG.

## 2. Preliminaries and setup

In this work, we delve into the task of crafting generative models for the purpose of sampling from the Boltzmann distribution driven by a predefined energy  $U : \mathbb{R}^d \rightarrow \mathbb{R}$ :

$$\pi(x) = \frac{1}{Z} \exp(-U(x)),$$

where the normalizing constant  $Z = \int \exp(-U(x))dx$  is usually computationally intractable. To tackle this challenge, the Boltzmann generator [18], along with its various extensions [24–26], has emerged as a prominent technique in

recent years. These approaches harness NF to parameterize a trainable and analytical density function, with parameter optimization achieved through the minimization of the KL divergence between the surrogate density and  $\pi$ . Nevertheless, in contrast to typical generative models, the pursuit of exact probability density computation imposes substantial constraints on NFs: Each transformation layer must be a bijection, and the determinant of its Jacobian matrix can be tractably computed. These requirements inherently limit the capacity of NFs to effectively model complex distributions.

Our focus now shifts to a generator akin to the VAE. This generator produces samples by a decoder as

$$x|z_0 \sim p_D(x|z_0, \phi),$$

where  $z_0 \sim p_D(z_0)$  is a latent variable drawn from a known prior distribution, typically a standard multivariate normal distribution. The parameter  $\phi$  characterizes the decoder, and we define  $p_D(x|z_0; \phi)$  as a Gaussian distribution  $\mathcal{N}(x|\mu(z_0; \phi), \Sigma(z_0; \phi))$ , with both  $\mu$  and  $\Sigma$  parameterized by neural networks (NNs). Similar to the VAE, we aim to train the networks  $\mu$  and  $\Sigma$  such that the marginal distribution  $p_D(x)$  of the generated samples aligns with the target distribution.

It is important to note that, unlike conventional data-driven VAEs, we do not have access to samples from the target distribution  $\pi(x)$ . In fact, obtaining such samples is precisely the goal of the generator. As a result, the variational approximation of the KL divergence  $D_{KL}(\pi(x)||p_D(x))$  cannot be used to train the model. Instead, in this work, we consider the following divergence and its upper bound:

$$\begin{aligned} D_{KL}(p_D(x)||\pi(x)) &\leq D_{KL}(p_D(z_0) \cdot p_D(x|z_0, \phi)||\pi(x) \cdot p_E(z_0|x, \theta)) \\ &= \mathbb{E}_{p_D(z_0) \cdot p_D(x|z_0, \phi)} \left[ \log \frac{p_D(z_0)p_D(x|z_0, \phi)}{p_E(z_0|x, \theta)} + U(x) \right] \\ &\quad + \log Z. \end{aligned} \tag{1}$$

Here, the parametric distribution  $p_E(z_0|x, \theta)$  defines an encoder that maps from  $x$  to the latent variable  $z$ , and the equality is achieved if  $p_E(z|x, \theta)$  matches the conditional distribution of  $z$  for a given  $x$ , deduced from the decoder.

It seems that we have only increased the complexity of the problem, as we are still required to approximate a conditional distribution. However, in the

upcoming section, we demonstrate that we can effectively construct the encoder using the diffusion model [35, 37] and optimize all parameters without the need to numerically solve ordinary or stochastic differential equations.

### 3. Energy-based diffusion generator

The diffusion model [37, 38] has emerged in recent years as a highly effective approach for estimating data distributions. Its core idea is to construct a diffusion process that progressively transforms data into simple white noise, and learn the reverse process to recover the data distribution from noise. In this work, we apply the principles of the diffusion model by incorporating a diffusion process into the latent space, enabling us to efficiently overcome the challenges arising from the variational framework for the sampling problem defined by Equation (1). We refer to the model produced by this method as the energy-based diffusion generator (EDG).

#### 3.1. Model architecture

In the EDG framework, we initiate a diffusion process from the latent variable  $z_0$  and combine it with the decoder, resulting in what we term the “decoding process”:

$$\begin{aligned} z_0 \in R^D &\sim p_D(z_0) \triangleq \mathcal{N}(x|0, I), & x|z_0 &\sim p_D(x|z_0; \phi) \\ dz_t &= f(z_t, t)dt + g(t)dW_t, & t &\in [0, T] \end{aligned} \quad (2)$$

where  $W_t$  is the standard Wiener process,  $f(\cdot, t) : R^D \rightarrow R^D$  acts as the drift coefficient, and  $g(\cdot) : R \rightarrow R$  serves as the diffusion coefficient. To streamline notation, we denote the probability distribution defined by the decoding process as  $p_D$ . In typical SDEs applied in diffusion models, two critical conditions hold: (a) the transition density  $p_D(z_t|z_0)$  can be analytically computed without numerically solving the Fokker-Planck equation, and (b)  $z_T$  is approximately uninformative with  $p_D(z_T) \approx p_D(z_T|z_0)$ .

If we only consider the statistical properties of the latent diffusion process  $z_{[\cdot]} = \{z_t\}_{t \in [0, T]}$ , it is uninformative and only describes a transition from one simple noise to another. However, when we account for the conditional distribution of  $z_t$  given a sample  $x$ , the process  $z_{[\cdot]}$  represents the gradual transformation of the complex conditional distribution  $p_D(z_0|x) \propto p_D(z_0) \cdot p_D(x|z_0)$  into the tractable distribution  $p_D(z_T|x) = p_D(z_T)$ , where the independence between  $z_T$  and  $x$  results from the independence between  $z_0$  and  $z_T$  (see

Appendix A). This implies that, starting from  $z_T \sim p_D(z_T)$ , we can obtain samples from  $p_D(z_0|x)$  by simulating the following reverse-time diffusion equation [45]:

$$dz_{\tilde{t}} = - \left( f(z_{\tilde{t}}, \tilde{t}) - g(\tilde{t})^2 \nabla_{z_{\tilde{t}}} \log p_D(z_{\tilde{t}}|x) \right) d\tilde{t} + g(\tilde{t}) dW_{\tilde{t}}, \quad (3)$$

where  $\tilde{t} = T - t$  denotes the reverse time. As in conventional diffusion models, practical implementation of this simulation is challenging due to the intractability of the score function  $\nabla_{z_{\tilde{t}}} \log p_D(z_{\tilde{t}}|x)$ , and we therefore also use a neural network to approximate the score function, denoted as  $s(z_{\tilde{t}}, x, \tilde{t}; \theta)$ . This approximation leads to what we refer to as the “encoding process”, achieved by integrating the parametric reverse-time diffusion process and the target distribution of  $x$ :

$$x \sim \pi(x), \quad z_T \sim p_E(z_T) \triangleq p_D(z_T) \\ dz_{\tilde{t}} = - \left( f(z_{\tilde{t}}, \tilde{t}) - g(\tilde{t})^2 s(z_{\tilde{t}}, x, \tilde{t}; \theta) \right) d\tilde{t} + g(\tilde{t}) dW_{\tilde{t}}, \quad \tilde{t} = T - t. \quad (4)$$

For simplicity of notation, we refer to the distribution defined by the encoding process as  $p_E$  in this paper.

Fig. 1 offers a visual depiction of the decoding and encoding processes. It is important to highlight that latent diffusion models, which are primarily designed to address generative modeling in data-driven scenarios, which have recently gained significant attention [46–48]. Their main idea is to use a pre-trained encoder and decoder to obtain a latent space that both effectively represents the data and facilitates efficient sampling, with the diffusion model learning the distribution of latent variables. Our model, EDG, leverages a similar idea to address energy-based sampling problems. The key differences between EDG and previous latent diffusion models in structure and algorithm are as follows: first, in EDG, the diffusion model itself functions as the encoder, eliminating the need for a separate encoder; second, by using a unified loss function, the decoder is trained jointly with the diffusion model (see Sec. 3.2).

Below, we present the construction details of modules in EDG, which are used in our experiments. In practical applications, more effective neural networks can be designed as needed.

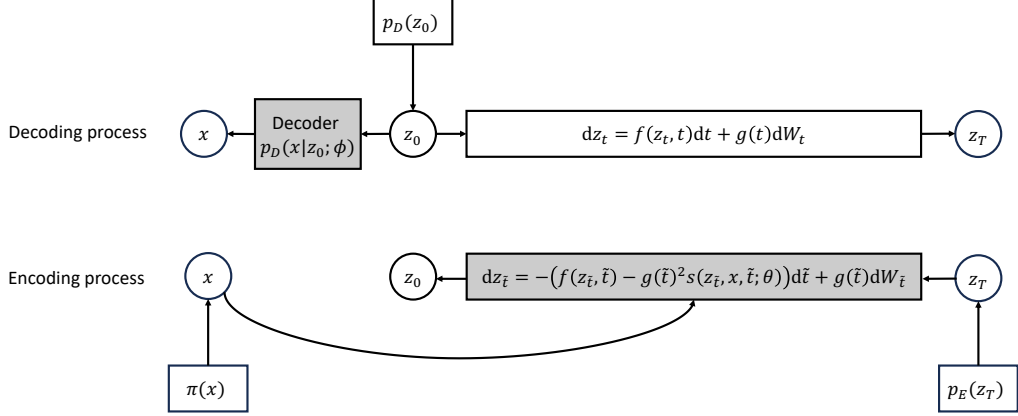


Figure 1: Probabilistic graphs of the decoding and encoding processes, highlighting the trainable parts of the model in gray.

### 3.1.1. Boundary condition-guided score function model

Considering that the true score function satisfies the following boundary conditions for  $t = 0, T$ :

$$\begin{aligned}
 \nabla_{z_0} \log p_D(z_0|x) &= \nabla_{z_0} [\log p_D(z_0|x) + \log p_D(x)] \\
 &= \nabla_{z_0} \log p_D(x, z_0) \\
 &= \nabla_{z_0} [\log p_D(x|z_0) + \log p_D(z_0)]
 \end{aligned}$$

and

$$\nabla_{z_T} \log p_D(z_T|x) = \nabla_{z_T} \log p_D(z_T),$$

we propose to express  $s(z, x, t; \theta)$  as

$$\begin{aligned}
 s(z, x, t; \theta) &= \left(1 - \frac{t}{T}\right) \cdot \nabla_{z_0} [\log p_D(x|z_0 = z) + \log p_D(z_0 = z)] \\
 &\quad + \frac{t}{T} \cdot \nabla_{z_T} \log p_D(z_T = z) + \frac{t}{T} \left(1 - \frac{t}{T}\right) s'(z, x, t; \theta),
 \end{aligned}$$

where  $s'(z, x, t; \theta)$  is the neural network to be trained. This formulation ensures that the error of  $s$  is zero for both  $t = 0$  and  $t = T$ .

### 3.1.2. Generalized Hamiltonian dynamics-based decoder

Inspired by generalized Hamiltonian dynamics (GHD) [12, 13], the decoder generates the output  $x$  using the following process. First, an initial

sample and velocity  $(y, v)$  are generated according to the latent variable  $z_0$ . Then,  $(y, v)$  is iteratively updated as follows:

$$\begin{aligned} v &:= v - \frac{\epsilon(l; \phi)}{2} \left( \nabla U(y) \odot e^{\frac{\epsilon_0}{2} Q_v(y, \nabla U(y), l; \phi)} + T_v(y, \nabla U(y), l; \phi) \right), \\ y &:= y + \epsilon(l; \phi) \left( v_k \odot e^{\epsilon_0 Q_y(v_k, l; \phi)} + T_y(v_k, l; \phi) \right), \\ v &:= v - \frac{\epsilon(l; \phi)}{2} \left( \nabla U(y) \odot e^{\frac{\epsilon_0}{2} Q_v(y, \nabla U(y), l; \phi)} + T_v(y, \nabla U(y), l; \phi) \right). \end{aligned}$$

Finally, the decoder output  $x$  is given by:

$$x = y - \exp(\epsilon_0 \eta(y; \phi)) \nabla U(y) + 2 \exp(\epsilon_0 \eta(y; \phi)) \xi$$

where  $\xi$  is distributed according to the standard Gaussian distribution. The equation can be interpreted as a finite-step approximation of Brownian dynamics  $dy = -\nabla U(y) dt + dW_t$ . In the above procedure,  $Q_v$ ,  $T_v$ ,  $Q_y$ ,  $T_y$ ,  $\epsilon$ , and  $\eta$  are all trainable neural networks.

The key advantages of the GHD-based decoder are twofold. First, it effectively leverages the gradient information of the energy function, and our experiments show that it can enhance the sampling performance for multimodal distributions. Second, by incorporating trainable correction terms and steps into the classical Hamiltonian dynamics, it achieves a good decoder density with only a few iterations. The complete decoding process can be found in Appendix C.

### 3.2. Loss function

To optimize parameters of the decoding and encoding processes, we can minimize the KL divergence between the joint distributions of  $(x, z_{[.]})$  provided by the decoding and encoding processes. The divergence is also an upper bound of  $D_{KL}(p_D(x) || \pi(x))$  like that in (1) due to the data processing inequality. As derived in Appendix B, the KL divergence can be expressed as

$$D_{KL}(p_D(x, z_{[.]}) || p_E(x, z_{[.]})) = \mathcal{L}(\theta, \phi) + \log Z, \quad (5)$$



where

$$\begin{aligned} \mathcal{L}(\theta, \phi) &= \mathbb{E}_{p_D} [\log p_D(x|z_0; \phi) + U(x)] \\ &+ \int_0^T \frac{g(t)^2}{2} \mathbb{E}_{p_D} \left[ \|s(z_t, x, t; \theta)\|^2 + 2\nabla_{z_t} \cdot s(z_t, x, t; \theta) \right. \\ &\left. + \|\nabla_{z_t} \log p_D(z_t)\|^2 \right] dt. \end{aligned} \quad (6)$$

By utilizing the importance-sampled integration and Hutchinson estimator, we can obtain an equivalent expression of  $\mathcal{L}(\theta, \phi)$ , which can be efficiently and unbiasedly estimated by Monte Carlo random sampling from  $p_D$  without numerical solutions to SDEs:

$$\begin{aligned} \mathcal{L}(\theta, \phi) &= \mathbb{E}_{p_D} [\log p_D(x|z_0; \phi) + U(x)] \\ &+ \int_0^T \lambda(t) \cdot \mathbb{E}_{p(t)p(\epsilon)p_D(x, z_t)} [\mathcal{L}_t(x, z_t, \epsilon; \theta)] dt, \end{aligned} \quad (7)$$

where

$$\mathcal{L}_t(x, z_t, \epsilon; \theta) = \|s(z_t, x, t; \theta)\|^2 + 2 \frac{\partial [\epsilon^\top s(z_t, x, t; \theta)]}{\partial z_t} \epsilon + \|\nabla_{z_t} \log p_D(z_t)\|^2,$$

$p(\epsilon)$  is the Rademacher distribution with  $\mathbb{E}[\epsilon] = 0, \text{cov}(\epsilon) = I$ ,  $p(t)$  is a proposal distribution of  $t \in [0, T]$ , and the weighting function  $\lambda(t) = \frac{g(t)^2}{2p(t)}$ . All neural networks involved in EDG can then be trained by minimizing the loss function (7) using stochastic gradient descent.

In our experiments, to mitigate the variance inherent in the Monte Carlo approximation of the loss function, we adopted the strategy from [49] to dynamically adjust the time proposal distribution  $p_D(t)$ , based on a historical buffer that stores recent loss values related to  $t$  in the r.h.s of (7). For more details, please refer to Appendix D.

### 3.3. Sample reweighting

After training, we can use the decoder  $p_D(x|z_0)$  to generate samples and compute various statistics of the target distribution  $\pi(x)$ . For example, for a quantity of interest  $O : \mathbb{R}^d \rightarrow \mathbb{R}$ , we can draw  $N$  augmented samples  $\{(x^n, z_0^n)\}_{n=1}^N$  from  $p_D(z_0)p_D(x|z_0)$  and estimate the expectation  $\mathbb{E}_{\pi(x)}[O(x)]$  as follows:

$$\mathbb{E}_{\pi(x)}[O(x)] \approx \frac{1}{N} \sum_n O(x^n).$$

However, due to model errors, this estimation can be systematically biased. To address this, we can apply importance sampling, using  $p_D(x, z_0) = p_D(z_0)p_D(x|z_0)$  as the proposal distribution and  $p_E(x, z_0) = \pi(x)p_E(z_0|x)$  as the augmented target distribution. We can then assign each sample  $(x, z_0)$  generated by the decoder an unnormalized weight:

$$w(x, z_0) = \frac{\exp(-U(x))p_E(z_0|x)}{p_D(z_0)p_D(x|z_0)} \propto \frac{\pi(x)p_E(z_0|x)}{p_D(z_0)p_D(x|z_0)} \quad (8)$$

and obtain a consistent estimate of  $\mathbb{E}_{\pi(x)}[O(x)]$  as:

$$\mathbb{E}_{\pi(x)}[O(x)] \approx \frac{\sum_n w(x^n, z_0^n)O(x^n)}{\sum_n w(x^n, z_0^n)},$$

where the estimation error approaches zero as  $N \rightarrow \infty$ .

In addition, the weight function  $w$  can also be used to estimate the normalizing constant  $Z$ , which is a crucial task in many applications, such as Bayesian model selection in statistics and free energy estimation in statistical physics. Based on (1), we have:

$$\log Z \geq -\mathbb{E}_{p_D(x, z_0)} [\log w(x, z_0)].$$

Here, the lower bound can also be estimated using samples from the decoder, and the tightness of this bound is achieved when  $p_D(x, z_0) = p_E(x, z_0)$ .

The main difficulty in above computations lies in the intractability of the marginal decoder density  $p_E(z_0|x)$  when calculating the weight function. To overcome this, following the conclusion from Sec. 4.3 in [37], we construct the following probability flow ordinary differential equation (ODE):

$$dz_t = \left( f(z_t, t) - \frac{1}{2}g(t)^2 s(z_t, x, t; \theta) \right) dt,$$

with the boundary condition  $z_T \sim p_E(z_T)$ . If  $s(z_t, x, t; \theta)$  accurately approximates the score function  $\nabla_{z_t} \log p_E(z_t|x)$  after training, the conditional distribution of  $z_t|x$  given by the ODE will match that of the encoding process for each  $t \in [0, 1]$ . Consequently, we can employ the neural ODE method [50] to efficiently compute  $p_E(z_0|x)$ .

## 4. Experiments

We conduct an empirical evaluation of EDG across a diverse range of energy functions. First, we present the results obtained from a set of two-dimensional distributions. Next, we showcase the performance of EDG in

the context of Bayesian Logistic regression. Last, we apply EDG to an Ising model. All the experimental details are provided in Appendix E. Additionally, we perform an ablation study to verify the effectiveness of each module in EDG. Please refer to Appendix F for more information.

In order to demonstrate the superiority of our model, we compare EDG with the following sampling methods:

- Vanilla Hamiltonian Monte Carlo method [8], denoted as V-HMC.
- L2HMC [13], a GHD-based MCMC method with a trainable proposal distribution model.
- Boltzmann Generator (BG) [18], a VI method where the surrogate distribution is modeled using RealNVP [51].
- Neural Renormalization Group (NeuralRG) [17], a method similar to BG and designed specifically for the Ising model. In this section, NeuralRG is only used for experiments of the Ising model.
- Path Integral Sampler (PIS) [39], a diffusion-based sampling model via numerical simulation of an SDE.

**2D energy function** Firstly, we compare our model with the other models on several synthetic 2D energy functions: MoG2(i) (Mixture of two isotropic Gaussians with the same  $\sigma^2 = 0.5$  or different variance  $\sigma_1^2 = 1.5, \sigma_2^2 = 0.3$  and centroids separated by distance 10), MoG6 (Mixture of six isotropic Gaussians with variance  $\sigma^2 = 0.1$ ), MoG9 (Mixture of nine

Table 1: The Maximum Mean Discrepancy (MMD) between the samples generated by each generator and the reference samples. Details on the calculation of discrepancy can be found in Appendix E.

	Mog2	Mog2(i)	Mog6	Mog9	Ring	Ring5
V-HMC	<b>0.01</b>	1.56	0.02	0.04	<b>0.01</b>	<b>0.01</b>
L2HMC	0.04	0.94	<b>0.01</b>	0.03	0.02	<b>0.01</b>
BG	1.90	1.63	2.64	0.07	0.05	0.18
PIS	<b>0.01</b>	1.66	<b>0.01</b>	0.42	<b>0.01</b>	0.78
<b>EDG</b>	<b>0.01</b>	<b>0.50</b>	<b>0.01</b>	<b>0.02</b>	<b>0.01</b>	0.02

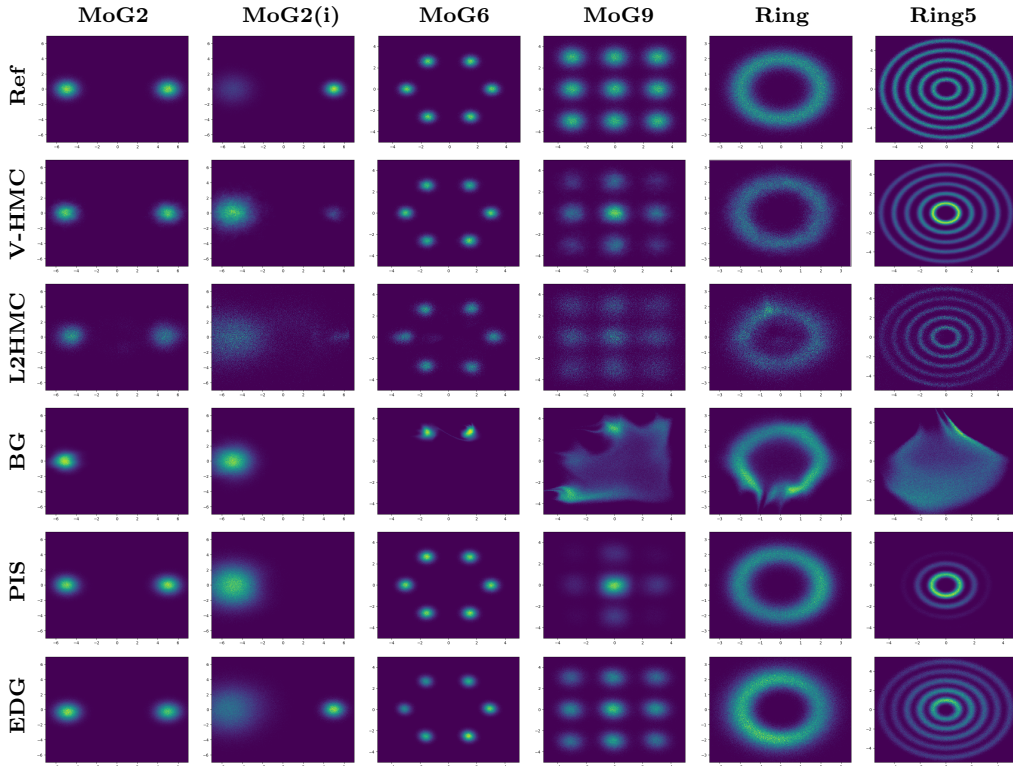


Figure 2: Density plots for 2D energy function. For the generation of reference samples, please refer to Appendix E. We generate 500,000 samples for each method and plot the histogram.

isotropic Gaussians with variance  $\sigma^2 = 0.3$ ), Ring, Ring5 (energy functions can be seen in [12]). We present the histogram of samples for visual inspection in Fig. 2, and Table 1 summarizes the sampling errors. As shown, EDG delivers higher-quality samples compared to the other methods. To elucidate the function of each component in EDG, we compare our model with vanilla VAE in Appendix F.

**Bayesian Logistic Regression** In the subsequent experiments, we highlight the efficacy of EDG in the context of Bayesian logistic regression, particularly when dealing with a posterior distribution residing in a higher-dimensional space. In this scenario, we tackle a binary classification problem with labels  $L = \{0, 1\}$  and high-dimensional features  $D$ . The classifier’s output is defined as

$$p(L = 1|D, x) = \text{softmax}(w^\top D + b),$$

Table 2: Classification accuracy and AUC results for Bayesian logistic regression tasks. The experiments utilize consistent training and test data partitions, where the HMC step size is set to 0.01. Average accuracy and AUC values, accompanied by their respective standard deviations, are computed across 32 independent experiments for all datasets.

	AU		GE		HE	
	Acc	Auc	Acc	Auc	Acc	Auc
V-HMC	82.97 ± 1.94	90.88 ± 0.83	78.52 ± 0.48	77.67 ± 0.28	86.75 ± 1.63	93.35 ± 0.76
L2HMC	73.26 ± 1.56	79.69 ± 3.65	62.02 ± 4.19	60.23 ± 5.10	82.23 ± 2.81	90.48 ± 0.51
BG	82.99 ± 1.18	91.23 ± 0.67	78.14 ± 1.44	77.59 ± 0.73	86.75 ± 1.99	93.44 ± 0.39
PIS	81.64 ± 2.63	91.23 ± 0.67	71.90 ± 3.17	71.67 ± 4.52	83.24 ± 3.95	91.68 ± 2.78
<b>EDG</b>	<b>84.96 ± 1.67</b>	<b>92.82 ± 0.69</b>	<b>79.40 ± 1.74</b>	<b>82.79 ± 1.46</b>	<b>88.02 ± 3.90</b>	<b>95.10 ± 1.23</b>

where  $x = (w, b)$ . We aim to draw samples  $x^1, \dots, x^N$  from the posterior distribution

$$\pi(x) \propto p(x) \prod_{(L,D) \in \mathcal{D}_{\text{train}}} p(L|D, x)$$

based on the training set  $\mathcal{D}_{\text{train}}$ , where the prior distribution  $p(x)$  is a standard Gaussian distribution. Then, for a given  $D$ , the conditional distribution  $p(L|D, \mathcal{D}_{\text{train}})$  can be approximated as  $\sum_n p(L|D, x^n)$ . We conduct experiments on three datasets: Australian (AU, 15 covariates), German (GE, 25 covariates), and Heart (HE, 14 covariates) [52], evaluating accuracy rate (ACC) and Area Under the Curve (AUC) on the test subset. Remarkably, as illustrated in Table 2, EDG consistently achieves the highest accuracy and AUC performance.

We extend our analysis to the binary Coverttype dataset comprising 581,012 data points and 54 features. The posterior of the classifier parameters follows a hierarchical Bayesian model (see Sec. 5 of [27]), with  $x$  denoting the combination of classifier parameters and the hyperparameter in the hierarchical Bayesian model. To enhance computational efficiency, in BG and EDG,  $\log \pi(x)$  is unbiasedly approximated during training as

$$\log \pi(x) \approx \log p(x) + \frac{|\mathcal{D}_{\text{train}}|}{|\mathcal{B}|} \sum_{(L,D) \in \mathcal{B}} \log p(L|D, x),$$

where  $\mathcal{B}$  is a random mini-batch. For V-HMC and L2HMC, the exact pos-

Table 3: Classification accuracy on the test dataset of Coverstype. The reported values represent averages and standard deviations of accuracy over 32 independent experiments.

	V-HMC	L2HMC	BG	PIS	<b>EDG</b>
Acc	49.88 $\pm$ 3.32	51.51 $\pm$ 3.46	50.75 $\pm$ 3.78	50.59 $\pm$ 2.94	<b>70.13 <math>\pm</math> 2.13</b>

terior density is calculated. As indicated by the results in Table 3, EDG consistently outperforms alternative methods.

**Ising model** Finally, we verify the performance of EDG on the 2-dimensional Ising model [17], a mathematical model of ferromagnetism in statistical mechanics. To ensure the continuity of physical variables, we employ a continuous relaxations trick [53] to transform discrete variables into continuous auxiliary variables with the target distribution:

$$\pi(\mathbf{x}) = \exp\left(-\frac{1}{2}\mathbf{x}^T (K(T) + \alpha I)^{-1} \mathbf{x}\right) \times \prod_{i=1}^N \cosh(x_i),$$

where  $K$  is an  $N \times N$  symmetric matrix depending on the temperature  $T$ ,  $\alpha$  is a constant guaranteeing  $K + \alpha I$  to be positive. For the corresponding discrete Ising variables  $\mathbf{s} = \{1, -1\}^{\otimes N}$ , one can directly obtain discrete samples

Table 4: The estimation of  $\log Z_{\text{Ising}}$  in 2D ising model with a dimension of 256 ( $16 \times 16$ ) is obtained by the method described in Sec. 3.3. We utilize a batch size of  $n = 256$  to estimate the mean and applies the central limit theorem to calculate the standard deviation of the mean of the statistic as  $\text{std}/\sqrt{n}$ .

$\log Z_{\text{Ising}}$	NeuralRG	PIS	<b>EDG</b>
$T = 2.0$	260 $\pm$ 0.13	210 $\pm$ 0.43	<b>270 <math>\pm</math> 0.18</b>
$T = 2.1$	250 $\pm$ 0.14	208 $\pm$ 0.41	<b>255 <math>\pm</math> 0.19</b>
$T = 2.2$	239 $\pm$ 0.16	210 $\pm$ 0.39	<b>252 <math>\pm</math> 0.17</b>
$T = 2.3$	231 $\pm$ 0.15	214 $\pm$ 0.37	<b>233 <math>\pm</math> 0.17</b>
$T = 2.4$	<b>225 <math>\pm</math> 0.17</b>	212 $\pm$ 0.37	<b>225 <math>\pm</math> 0.15</b>
$T = 2.5$	219 $\pm$ 0.17	202 $\pm$ 0.37	<b>221 <math>\pm</math> 0.14</b>
$T = 2.6$	<b>216 <math>\pm</math> 0.18</b>	181 $\pm$ 0.40	214 $\pm$ 0.14
$T = 2.7$	<b>212 <math>\pm</math> 0.18</b>	189 $\pm$ 0.36	<b>212 <math>\pm</math> 0.14</b>

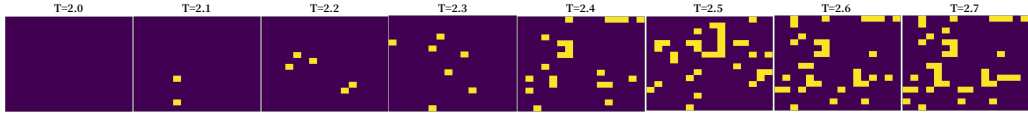


Figure 3: The generated states at different temperatures from  $T = 2.0$  to  $T = 2.7$  by EDG with a dimensionality of 256 ( $16 \times 16$ ), where the latent variable  $z_0$  remains fixed. As the temperature rises, the model’s state tends progressively toward disorder.

according to  $\pi(\mathbf{s}|\mathbf{x}) = \prod_i (1 + e^{-2s_i x_i})^{-1}$ . When there is no external magnetic field and each spin can only interact with its neighboring spins,  $K$  is defined as  $\sum_{\langle ij \rangle} s_i s_j / T$ , with the nears neighboring sum  $\langle ij \rangle$ . Consequently, the normalizing constant of the continuous relaxations system is given by  $\log Z = \log Z_{\text{Ising}} + \frac{1}{2} \ln \det(K + \alpha I) - \frac{N}{2} [\ln(2/\pi) - \alpha]$  [17]. Additionally, using the method described in Sec. 3.3, we provide lower bound estimates of  $\log Z_{\text{Ising}}$  at different temperatures for samples generated by NeuralRG, PIS and EDG. Since these are lower bound estimates, larger values indicate more accurate results. As seen in Table 4, EDG provides the most accurate estimates of  $\log Z$  across most temperature ranges. The generated states at different temperatures are displayed in Fig. 3.

## 5. Conclusion

In summary, our work introduces the EDG as an innovative and effective sampling approach by combining principles from VI and diffusion based methods. Drawing inspiration from VAEs, EDG excels in efficiently generating samples from intricate Boltzmann distributions. Leveraging the expressive power of the diffusion model, our method accurately estimates the KL divergence without the need for numerical solutions to ordinary or stochastic differential equations. Empirical experiments validate the superior sampling performance of EDG.

In consideration of its powerful generation ability and unrestrained network design theoretically, there is still room for further exploration. We can design specific network architectures for different tasks and find the most elaborate one. Nevertheless, it is the first attempt to design a one-shot generator assisted by diffusion models.

In future, our primary focus will be on extending the application of EDG to construct generative models for large-scale physical and chemical systems, such as proteins [54, 55].

## Acknowledgements

The first and third authors are supported by the NSF of China (under grant number 12171367). The second author is supported by the NSF of China (under grant numbers 92270115, 12071301) and the Shanghai Municipal Science and Technology Commission (No. 20JC1412500), and Henan Academy of Sciences. The last author was supported by the NSF of China (No. 12288201), the Strategic Priority Research Program of Chinese Academy of Sciences (Grant No. XDA25010404), the National Key R&D Program of China (2020YFA0712000), the Youth Innovation Promotion Association, CAS, and Henan Academy of Sciences.

## Appendix A. Proof of the independence between $z_T$ and $x$

In the decoding process, if  $z_T$  is independent of  $z_0$ , we have

$$\begin{aligned} p_D(z_T|x) &= \int p_D(z_T|z_0)p_D(z_0|x)dz_0 \\ &= p_D(z_T) \cdot \int p_D(z_0|x)dz_0 \\ &= p_D(z_T). \end{aligned}$$

## Appendix B. Proof of (5)

For an extremely small lag time  $\tau$ , the Euler-Maruyama discretization of  $z_{[\cdot]}$  in the decoding process provides

$$z_t = z_{t-\tau} + f(z_{t-\tau}, t - \tau)\tau + \sqrt{\tau}g(t - \tau)u_{t-\tau}, \quad (\text{B.1})$$

$$z_{t-\tau} = z_t - \left( f(z_t, t) - g(t)^2 \nabla \log p_D(z_t) \right) \tau + \sqrt{\tau}g(t)\bar{u}_t, \quad (\text{B.2})$$

where  $u_{t-\tau}, \bar{u}_t \sim \mathcal{N}(\cdot|0, I)$ . Importantly,  $u_{t-\tau}$  is independent of  $\{z_{t'}|t' \leq t - \tau\}$  and  $x$ , and  $\bar{u}_t$  is independent of  $\{z_{t'}|t' \geq t\}$ . The Euler-Maruyama approximation of  $p_E(z_{[\cdot]}|x)$  gives

$$z_{t-\tau} = z_t - \left( f(z_t, t) - g(t)^2 s(z_t, x, t) \right) \tau + \sqrt{\tau}g(t)v_t \quad (\text{B.3})$$

with  $v_t \sim \mathcal{N}(\cdot|0, I)$ .

According to (B.2, B.3), we can obtain



$$\begin{aligned}
\mathbb{E}_{p_D} [\log p_D(z_{t-\tau}|z_t)] &= -\frac{d}{2} \log 2\pi - \frac{d}{2} \log \tau g(t)^2 \\
&\quad - \frac{1}{2} \tau^{-1} g(t)^{-2} \mathbb{E}_{p_D} \left[ \left\| z_{t-\tau} - z_t + (f(z_t, t) - g(t)^2 \nabla \log p_D(z_t)) \tau \right\|^2 \right] \\
&= -\frac{d}{2} \log 2\pi - \frac{d}{2} \log \tau g(t)^2 - \frac{1}{2} \tau^{-1} g(t)^{-2} \mathbb{E}_{p_D} \left[ \left\| \sqrt{\tau} g(t) \bar{u}_t \right\|^2 \right] \\
&= -\frac{d}{2} \log 2\pi - \frac{d}{2} \log \tau g(t)^2 - \frac{d}{2} \tag{B.4}
\end{aligned}$$

and

$$\begin{aligned}
\mathbb{E}_{p_D} [\log p_E(z_{t-\tau}|z_t, x)] &= -\frac{d}{2} \log 2\pi - \frac{d}{2} \log \tau g(t)^2 \\
&\quad - \frac{1}{2} \tau^{-1} g(t)^{-2} \mathbb{E}_{p_D} \left[ \left\| z_{t-\tau} - z_t + (f(z_t, t) - g(t)^2 s(z_t, x)) \tau \right\|^2 \right] \\
&= -\frac{d}{2} \log 2\pi - \frac{d}{2} \log \tau g(t)^2 \\
&\quad - \frac{1}{2} \tau^{-1} g(t)^{-2} \mathbb{E}_{p_D} \left[ \left\| z_{t-\tau} - z_t + f(z_t, t) \tau \right\|^2 \right] \\
&\quad - \frac{1}{2} \tau^{-1} g(t)^{-2} \mathbb{E}_{p_D} \left[ \left\| g(t)^2 s(z_t, x) \tau \right\|^2 \right] \\
&\quad + \tau^{-1} g(t)^{-2} \mathbb{E}_{p_D} \left[ (z_{t-\tau} - z_t + f(z_t, t) \tau)^\top g(t)^2 s(z_t, x) \tau \right] \\
&= -\frac{d}{2} \log 2\pi - \frac{d}{2} \log \tau g(t)^2 \\
&\quad - \frac{1}{2} \tau^{-1} g(t)^{-2} \mathbb{E}_{p_D} \left[ \left\| g(t)^2 \nabla \log p_D(z_t) \tau + \sqrt{\tau} g(t) \bar{u}_t \right\|^2 \right] \\
&\quad - \frac{1}{2} \tau g(t)^2 \mathbb{E}_{p_D} \left[ \left\| s(z_t, x) \right\|^2 \right] \\
&\quad + \mathbb{E}_{p_D} \left[ (z_{t-\tau} - z_t + f(z_t, t) \tau)^\top s(z_t, x) \right] \\
&\stackrel{(i)}{=} -\frac{d}{2} \log 2\pi - \frac{d}{2} \log \tau g(t)^2 - \frac{d}{2} \\
&\quad - \frac{1}{2} \tau g(t)^2 \mathbb{E}_{p_D} \left[ \left\| \nabla \log p_D(z_t) \right\|^2 \right] \\
&\quad - \frac{1}{2} \tau g(t)^2 \mathbb{E}_{p_D} \left[ \left\| s(z_t, x) \right\|^2 \right] \\
&\quad + \mathbb{E}_{p_D} \left[ (z_{t-\tau} - z_t + f(z_t, t) \tau)^\top s(z_t, x) \right], \tag{B.5}
\end{aligned}$$

where (i) results from the independence between  $\bar{u}_t$  and  $z_t$ .

By using (B.1) and the first-order Taylor expansion, we have

$$\begin{aligned}
z_{t-\tau} - z_t + f(z_t, t)\tau &= z_{t-\tau} - \left( z_{t-\tau} + f(z_{t-\tau}, t - \tau)\tau + \sqrt{\tau}g(t - \tau)u_{t-\tau} \right) \\
&\quad + f\left( z_{t-\tau} + f(z_{t-\tau}, t)\tau + \sqrt{\tau}g(t - \tau)u_{t-\tau}, t \right)\tau \\
&= -f(z_{t-\tau}, t - \tau)\tau - \sqrt{\tau}g(t - \tau)u_{t-\tau} \\
&\quad + \tau f(z_{t-\tau}, t - \tau) \\
&\quad + \tau \frac{\partial f(z_{t-\tau}, t - \tau)}{\partial z_{t-\tau}} (z_t - z_{t-\tau}) \\
&\quad + \tau^2 \frac{\partial f(z_{t-\tau}, t - \tau)}{\partial t} \\
&\quad + \tau \cdot O\left(\|z_t - z_{t-\tau}\|^2 + \tau^2\right) \\
&= -\sqrt{\tau}g(t - \tau)u_{t-\tau} \\
&\quad + \tau \frac{\partial f(z_{t-\tau}, t - \tau)}{\partial z_{t-\tau}} \left( f(z_{t-\tau}, t - \tau)\tau + \sqrt{\tau}g(t - \tau)u_{t-\tau} \right) \\
&\quad + \tau^2 \frac{\partial f(z_{t-\tau}, t - \tau)}{\partial t} \\
&\quad + \tau \cdot O\left(\left\|f(z_{t-\tau}, t - \tau)\tau + \sqrt{\tau}g(t - \tau)u_{t-\tau}\right\|^2 + \tau^2\right) \\
&= -\sqrt{\tau}g(t - \tau)u_{t-\tau} + O(\tau^2)
\end{aligned}$$

and

$$\begin{aligned}
s(z_t, x, t) &= s(z_{t-\tau}, x, t - \tau) + \frac{\partial s(z_{t-\tau}, x, t - \tau)}{\partial z_{t-\tau}} (z_t - z_{t-\tau}) + \frac{\partial s(z_{t-\tau}, x, t - \tau)}{\partial t} \tau \\
&= s(z_{t-\tau}, x, t - \tau) \\
&\quad + \frac{\partial s(z_{t-\tau}, x, t - \tau)}{\partial z_{t-\tau}} \left( f(z_{t-\tau}, t - \tau)\tau + \sqrt{\tau}g(t - \tau)u_{t-\tau} \right) \\
&\quad + \frac{\partial s(z_{t-\tau}, x, t - \tau)}{\partial t} \tau \\
&= s(z_{t-\tau}, x, t - \tau) + \sqrt{\tau} \frac{\partial s(z_{t-\tau}, x, t - \tau)}{\partial z_{t-\tau}} g(t - \tau)u_{t-\tau} + O(\tau).
\end{aligned}$$

Combining the two equations above, we get

$$\begin{aligned}
\mathbb{E}_{p_D} \left[ (z_{t-\tau} - z_t + f(z_t, t)\tau)^\top s(z_t, x, t) \right] &= \mathbb{E}_{p_D} \left[ -\sqrt{\tau}g(t-\tau)u_{t-\tau}^\top s(z_{t-\tau}, x, t-\tau) \right] \\
&\quad - \tau g(t-\tau)^2 \mathbb{E}_{p_D} \left[ u_{t-\tau}^\top \frac{\partial s(z_{t-\tau}, x, t-\tau)}{\partial z_{t-\tau}} u_{t-\tau} \right] \\
&\quad + o(\tau) \\
&\stackrel{(ii)}{=} -\tau g(t-\tau)^2 \mathbb{E}_{p_D} \left[ \text{tr} \left( \frac{\partial s(z_{t-\tau}, x, t-\tau)}{\partial z_{t-\tau}} \right) \right] \\
&\quad + o(\tau), \tag{B.6}
\end{aligned}$$

where (ii) follows from the fact that  $u_{t-\tau}$  is independent of  $z_{t-\tau}$  and  $x$  in the decoding process. Taking into account (B.6), (B.4) and (B.5), we arrive at the following results:

$$\begin{aligned}
\Delta_t &\triangleq \mathbb{E}_{p_D} [\log p_D(z_{t-\tau}|z_t)] - \mathbb{E}_{p_D} [\log p_E(z_{t-\tau}|z_t, x)] \\
&= \frac{1}{2} \tau g(t)^2 \mathbb{E}_{p_D} [\|\nabla \log p_D(z_t)\|^2] \\
&\quad + \frac{1}{2} \tau g(t)^2 \mathbb{E}_{p_D} [\|s(z_t, x, t)\|^2] \\
&\quad + \tau g(t-\tau)^2 \mathbb{E}_{p_D} \left[ \text{tr} \left( \frac{\partial s(z_{t-\tau}, x, t-\tau)}{\partial z_{t-\tau}} \right) \right] + o(\tau).
\end{aligned}$$

Let  $\tau = T/L$ , where  $L$  is a large number, we have

$$\begin{aligned}
\mathbb{E}_{p_D} \left[ \log \frac{p_D(x, z_0, z_\tau, \dots, z_T)}{p_E(x, z_0, z_\tau, \dots, z_T)} \right] &= \mathbb{E}_{p_D} \left[ \log \frac{p_D(x|z_0)p_D(z_T) \prod_{l=1}^L p_D(z_{(l-1)\tau}|z_{l\tau})}{\pi(x)p_E(z_T) \prod_{l=1}^L p_E(z_{(l-1)\tau}|z_{l\tau}, x)} \right] \\
&= \mathbb{E}_{p_D} \left[ \log \frac{p_D(x|z_0)}{Z^{-1} \exp(-U(x))} \right] + \sum_{l=1}^L \Delta_{l\tau} \\
&= \mathbb{E}_{p_D} [\log p_D(x|z_0) + U(x)] + \log Z + \sum_{l=1}^L \Delta_{l\tau}
\end{aligned}$$

and

$$\begin{aligned}
\mathbb{E}_{p_D} \left[ \log \frac{p_D(x, z_{[\cdot]})}{p_E(x, z_{[\cdot]})} \right] &= \lim_{L \rightarrow \infty} \mathbb{E}_{p_D} \left[ \log \frac{p_D(x, z_0, z_\tau, \dots, z_T)}{p_E(x, z_0, z_\tau, \dots, z_T)} \right] \\
&= \mathbb{E}_{p_D} [\log p_D(x|z_0) + U(x)] \\
&\quad + \int \frac{g(t)^2}{2} \mathbb{E}_{p_D} \left[ \|s(z_t, x, t)\|^2 + 2\text{tr} \left( \frac{\partial s(z_t, x, t)}{\partial z_t} \right) + \|\nabla \log p_D(z_t)\|^2 \right] dt \\
&\quad + \log Z.
\end{aligned}$$

Considering integration by parts,  $D_{KL}(p_D||p_E)$  in Eq.(6) has the following equivalent expression

$$\begin{aligned}
\mathbb{E}_{p_D} \left[ s(z_t, x)^\top \nabla_{z_t} \log p_D(z_t|z_0) | x, z_0 \right] &= \int p_D(z_t|z_0) s(z_t, x)^\top \nabla_{z_t} \log p_D(z_t|z_0) dz_t \\
&= \int s(z_t, x)^\top \nabla_{z_t} p_D(z_t|z_0) dz_t \\
&= \int \operatorname{div}_{z_t} (p_D(z_t|z_0) s(z_t, x)) dz_t \\
&\quad - \int p_D(z_t|z_0) \operatorname{tr} \left( \frac{\partial s(z_t, x)}{\partial z_t} \right) dz_t \\
&= -\mathbb{E}_{p_D} \left[ \operatorname{tr} \left( \frac{\partial s(z_t, x)}{\partial z_t} \right) | z_0 \right] \\
\Rightarrow \mathbb{E}_{p_D} \left[ s(z_t, x)^\top \nabla_{z_t} \log p_D(z_t|z_0) \right] &= -\mathbb{E}_{p_D} \left[ \operatorname{tr} \left( \frac{\partial s(z_t, x)}{\partial z_t} \right) \right]
\end{aligned}$$

Substituting the above equation to Eq.(6), we have

$$\begin{aligned}
D_{KL}(p_D(x, z_{[.]})||p_E(x, z_{[.]})) &= \mathbb{E}_{p_D} \left[ \log \frac{p_D(x|z_0; \phi)}{\pi(x)} \right] \\
&\quad + \mathbb{E}_{p_D} \left[ \frac{g^2(t)}{2} \left( \|\nabla \log p_D(z_t)\|^2 + \|s(z_t, x, t|\theta)\|^2 \right. \right. \\
&\quad \left. \left. - 2s(z_t, x, t|\theta)^\top \nabla \log p_D(z_t|z_0) \right) \right].
\end{aligned}$$

### Appendix C. Implementation of decoder

The detailed implementation of the GHD based decoder is summarized in Algorithm 1. Within the algorithm, we initially stochastically generate a sample  $y$  using the random variable  $\zeta$  (refer to Line 1 of the algorithm). Subsequently, we iteratively update the sample using random velocities  $v_1, \dots, v_K$  and GHD (see Line 5). Finally, we utilize discretized Brownian dynamics with a trainable step size to design the decoder density of  $x$  (refer to Line 9). Here,  $\epsilon(l; \phi)$ ,  $Q_v$ ,  $Q_y$ ,  $T_v$  and  $T_y$  are all neural networks composed of three-layer MLPs.  $\epsilon_0$  serves as a hyperparameter, and our numerical experiments suggest that setting  $\epsilon_0$  to a small positive value can improve the stability of the algorithm.

---

**Algorithm 1** GHD based decoder

---

**Require:**  $z_0 = (\zeta, v_1, \dots, v_K)$  drawn from the standard Gaussian distribution and decoder parameters  $\phi$

- 1: Let  $y := a(\zeta; \phi)$ .
- 2: **for**  $k = 1, \dots, K$  **do**
- 3:     **for**  $j = 1, \dots, J$  **do**
- 4:         Let  $l :=$  leap frog step of GHD.
- 5:         Udata  $(y, v_i)$  by

$$v_k := v_k - \frac{\epsilon(l; \phi)}{2} \left( \nabla U(y) \odot e^{\frac{\epsilon_0}{2} Q_v(y, \nabla U(y), l; \phi)} + T_v(y, \nabla U(y), l; \phi) \right)$$

$$y := y + \epsilon(l; \phi) \left( v_k \odot e^{\epsilon_0 Q_y(v_k, l; \phi)} + T_y(v_k, l; \phi) \right)$$

$$v_k := v_k - \frac{\epsilon(l; \phi)}{2} \left( \nabla U(y) \odot e^{\frac{\epsilon_0}{2} Q_v(y, \nabla U(y), l; \phi)} + T_v(y, \nabla U(y), l; \phi) \right)$$

- 6:     **end for**
  - 7:     Let  $v_k := -v_k$ .
  - 8: **end for**
  - 9: Let  $\mu = y - e^{\epsilon_0 \eta(y; \phi')} \nabla U(y)$  and  $\Sigma = 2e^{\epsilon_0 \eta(y; \phi')} I$ .
  - 10: **return**  $x \sim \mathcal{N}(\mu, \Sigma)$ .
- 

## Appendix D. Importance weighting for accurate time integral

It can be seen from (7) that an ideal choice for the time proposal  $p(t)$  in Monte Carlo estimation of the integral on the right-hand side is given by

$$p(t) \propto g^2(t) \mathbb{E}_{p(\epsilon) p_D(x, z_t)} [\mathcal{L}_t(x, z_t, \epsilon; \theta)].$$

In our experiments, we approximate the ideal proposal using the strategy introduced in [49]. The implementation details are as follows: We maintain a history buffer containing values of  $\mathcal{L}_t$  from the most recent 30 minibatches. In each iteration, the buffer provides an estimate of the expected value of  $\mathcal{L}_t$  as a function of  $t$  using a histogram with 100 bins over the time interval  $[0, T]$ . Subsequently, we obtain an estimate of the ideal  $p(t)$  for each iteration. Initially, during the early stages of training,  $p(t)$  is set as a uniform distribution until  $B_{\text{buffer}}$  minibatches are accumulated.

## Appendix E. Experimental details

**EDG** In our experiments, we leverage the subVP SDE proposed in [37] to model the diffusion process of  $z_t$  in (2), defined as

$$dz_t = -\frac{1}{2}\beta(t)z_t dt + \sqrt{\beta(t)\left(1 - e^{-2\int_0^t \beta(s)ds}\right)}dW_t$$

with  $T = 1$ . Here,  $\beta(t) = \beta_{\min} + t(\beta_{\max} - \beta_{\min})$ , and we set  $\beta_{\min} = 0.1$  and  $\beta_{\max} = 20$  for experiments. The initial state  $z_0$  follows a standard Gaussian distribution. Line 1 of Algorithm 1 is implemented as

$$y := \mu_0(\zeta_0; \phi) + \Sigma_0(\zeta_0; \phi)\zeta_1,$$

where  $\zeta = (\zeta_0, \zeta_1)$ , and  $\mu_0(\zeta_0; \phi), \Sigma_0(\zeta_0; \phi)$  are modeled by MLPs. When incorporating the GHD in the decoder, we set  $K = 5$  and  $J = 5$ .

**Baseline** For V-HMC, we facilitate the generation of samples after a warm-up phase comprising 1,000 steps, where each step the Metropolis-Hastings acceptance probability is computed to ensure the convergence. For L2HMC, we use a three-layer fully connected network, setting the leapfrog step length to 10. For different tasks, we adaptively select varying step sizes. For PIS, we use the publicly available code on our tasks directly. Regarding BG, the RealNVP architecture consists of 3 affine blocks, where the scaling and translation functions are modeled by a three-layer fully connected network, each with 256 units and ReLU activation functions.

**2D energy function** We use the following model architectures to generate samples for 2D energy tasks. ‘fc  $n$ ’ denotes a fully connected layer with  $n$  neurons.

The model architecture of 2D energy tasks

Decoding process	Encoding process
Network $a(\zeta; \phi)$ :	Score network:
fc $10 \times 32$ , ReLU, $2 \times (\text{fc } 32 \times 32, \text{ ReLU}), \text{ fc } 32 \times 2$ .	fc $25 \times 16$ , ReLU,
GHD:	fc $16 \times 16$ , ReLU,
$Q_v, T_v$ :	fc $16 \times 22$ .
fc $5 \times 10$ , Tanh, fc $10 \times 10$ , Tanh, fc $10 \times 2$ .	
$Q_x, T_x$ :	
fc $3 \times 10$ , ReLU, fc $10 \times 10$ , ReLU, fc $10 \times 2$ .	
Final network $N(\mu, \Sigma)$ :	
fc $2 \times 10$ , ReLU, fc $10 \times 10$ , ReLU, fc $10 \times 2$ .	

Reference samples for Mog2, Mog2(i), Mog6, and Mog9 in Fig. 2 are precisely drawn from the target distributions, as these distributions are mixtures of Gaussian distributions. Reference samples for Ring and Ring5 are generated using the Metropolis-Hastings algorithm, with a large number of iterations. Gaussian distributions with variances of 9 and 25, respectively, are used as the proposal distributions. For the V-HMC, we employ the use of an HMC run of a total length of 2,000 steps, initiating from a standard normal distribution. The first 1,000 steps are designated as burn-in steps followed by a subsequent 1,000 steps used for sample generation. This procedure is independently executed 500 times for the purpose of creating the visual representation.

Given the reference samples  $X = \{x_i\}_{i=1}^m$  and the generated samples  $Y = \{y_i\}_{i=1}^m$ , the Maximum Mean Discrepancy (MMD) [56] measures the difference between the distributions of  $X$  and  $Y$  as follows:

$$\text{MMD}^2(X, Y) = \frac{1}{m(m-1)} \sum_i \sum_{j \neq i} k(x_i, x_j) - \frac{2}{m^2} \sum_i \sum_j k(x_i, y_j) + \frac{1}{m(m-1)} \sum_i \sum_{j \neq i} k(y_i, y_j)$$

where  $k(\cdot, \cdot)$  denotes the kernel function to compute the inner product. RBF kernel is used in Table 1, and the bandwidth is set as the median distance between corresponding samples. We execute 20 cycles for each model to procure 5,000 desired samples, following which we evaluate the mean value of MMD in relation to 5,000 reference data. The standard deviations are all small, hence we do not report them in the table.

The model architecture of Bayesian Logistic Regression

Decoding process	Encoding process
Network $a(\zeta; \phi)$ : fc $d \times 256$ , ReLU, $2 \times (\text{fc } 256 \times 256, \text{ReLU})$ , fc $256 \times 256$ .	Score network: fc $(12d + 1) \times 256$ , ReLU,
GHD: $Q_v, T_v$ : fc $(2d + 1) \times 256$ , Tanh, fc $256 \times 256$ , Tanh, fc $256 \times d$ .	fc $256 \times 256$ , ReLU, fc $256 \times 11d$ .
$Q_x, T_x$ : fc $(d + 1) \times 256$ , ReLU, fc $256 \times 256$ , ReLU, fc $256 \times d$ .	
Final network $N(\mu, \Sigma)$ : fc $11d \times 256$ , ReLU, fc $256 \times 256$ , ReLU, fc $256 \times d$ .	

**Bayesian Logistic Regression** In all experiments, we employ the same data partition and the datasets are divided into training and test sets at a ratio of 4:1. Before training, we normalize all datasets to have zero mean

and unit variance. For  $d$ -dimensional features, the architectures of neural networks involved in the EDG are as follows:

In the task of covertime,  $x = (\alpha, w, b)$  with the prior distribution  $p(x) = p(\alpha)p(w, b|\alpha)$ , where  $p(\alpha) = \text{Gamma}(\alpha; 1, 0.01)$  and  $p(w, b|\alpha) = \mathcal{N}(w, b; 0, \alpha^{-1})$ .

**Ising model** The model architecture is shown below, which is similar to that in NeuralRG [17] without stacking bijectors to form a reversible transformation. It retains the multiscale entanglement renormalization ansatz structure, while we only use one block to update the whole dimensions of the variable directly.

The model architecture of Ising model	
Decoding process	Encoding process
Network $a(\zeta; \phi)$ : hierarchy network as shown in [17]	Score network: hierarchy network.
GHD: $Q_v, T_v$ : Conv2d $2 \times 10$ , BatchNorm2d, ReLU, Conv2d $10 \times 1$ . $Q_x, T_x$ : Conv2d $1 \times 10$ , BatchNorm2d, ReLU, Conv2d $10 \times 1$ .	Input: $z_t, x, t, T$
Final network $N(\mu, \Sigma)$ : fc $d \times 10$ , ReLU, fc $10 \times 10$ , ReLU, fc $10 \times d$ .	

Regarding the  $p_E(z_0|x, \theta^*)$ , we employ the RK45 ODE solver implemented in `scipy.integrate.solve_ivp`, where the parameters set identical to those in [37]. The normalizing constant  $\log Z$  is approximated according to Sec. 3.3.

## Appendix F. Ablation study

To elucidate the function of each component in EDG, we compare the following models on the sampling task of 2D energy functions: a VAE with the Gaussian decoder and encoder, where the means and diagonal covariance matrices are both parameterized by MLPs; a VAE with a GHD-based decoder and MLP-based encoder; EDG without GHD, where the decoder is modeled by MLPs; and the full EDG model. For VAE w/o GHD, the network is composed of 3-layer MLPs, each with 32 units and ReLU activation function. Starting from  $z \sim N(0, I_d)$ ,  $d = 10$ , the decoder generates samples  $x \sim p_D(x; \mu(z; \phi), \Sigma(z; \phi))$ . The encoder, as an independent network, follows  $p_E(z|x) = N(z; \mu(x; \theta), \Sigma(x; \theta))$ . The objective function is the KL divergence



of the joint distribution of  $z$  and  $x$  as

$$D_{\text{KL}}(p_D(z)p_D(x|z; \phi) || \pi(x)p_E(z|x; \theta)).$$

For VAE w/ GHD, the decoder is consistent with the structure in Algorithm 1, and the encoder is the same as described above. For EDG w/o GHD, we omit the leap-frog component (refer to Line 2-8 in the algorithm) and the decoder is composed of the network  $a(\zeta; \phi)$  and a final gaussian part  $\mathcal{N}(\mu, \Sigma)$  (refer to Line 1, 9 in the algorithm).

The histograms of the samples are shown in Fig. F.4 for visual inspection and the sampling errors is summarized in Tab. F.5. It is evident that EDG with a GHD-based decoder outperforms the other methods, demonstrating the effectiveness of each component within the model.

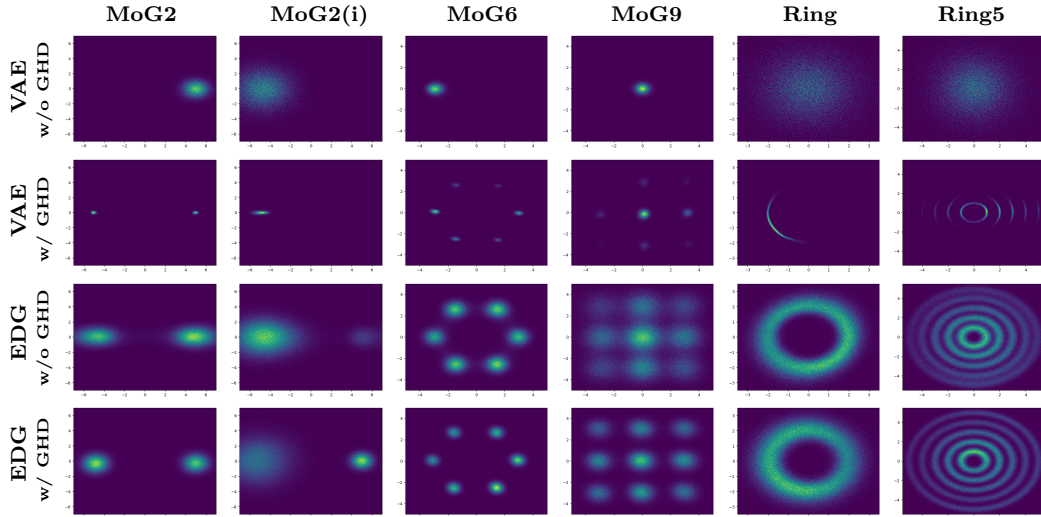


Figure F.4: Density plots for 2D energy function. We generate 500,000 samples for each method and plot the histogram.

Table F.5: The Maximum Mean Discrepancy (MMD) between 5,000 samples generated by each generator and the reference samples.

	Mog2	Mog2(i)	Mog6	Mog9	Ring	Ring5
<b>VAE w/o GHD</b>	1.86	1.62	2.57	2.10	0.12	0.23
<b>VAE w/ GHD</b>	<b>0.01</b>	2.43	0.15	0.59	1.68	0.63
<b>EDG w/o GHD</b>	0.06	1.01	0.04	0.05	0.02	0.04
<b>EDG</b>	<b>0.01</b>	<b>0.50</b>	<b>0.01</b>	<b>0.02</b>	<b>0.01</b>	0.02

## References

- [1] Y. I. Yang, Q. Shao, J. Zhang, L. Yang, Y. Q. Gao, Enhanced sampling in molecular dynamics, *The Journal of chemical physics* 151 (2019).
- [2] J. Hénin, T. Lelièvre, M. R. Shirts, O. Valsson, L. Delemotte, Enhanced sampling methods for molecular dynamics simulations, *arXiv preprint arXiv:2202.04164* (2022).
- [3] D. Maclaurin, R. P. Adams, Firefly monte carlo: Exact mcmc with subsets of data, *arXiv preprint arXiv:1403.5693* (2014).
- [4] P. W. Glynn, C.-h. Rhee, Exact estimation for markov chain equilibrium expectations, *Journal of Applied Probability* 51 (2014) 377–389.
- [5] K. Binder, E. Luijten, Monte carlo tests of renormalization-group predictions for critical phenomena in ising models, *Physics Reports* 344 (2001) 179–253.
- [6] N. Walker, K.-M. Tam, M. Jarrell, Deep learning on the 2-dimensional ising model to extract the crossover region with a variational autoencoder, *Scientific reports* 10 (2020) 13047.
- [7] W. K. Hastings, Monte carlo sampling methods using markov chains and their applications, *Biometrika* (1970).
- [8] R. M. Neal, et al., Mcmc using hamiltonian dynamics, *Handbook of markov chain monte carlo* 2 (2011) 2.
- [9] T. Araki, K. Ikeda, Adaptive markov chain monte carlo for auxiliary variable method and its application to parallel tempering, *Neural Networks* 43 (2013) 33–40.
- [10] T. Araki, K. Ikeda, S. Akaho, An efficient sampling algorithm with adaptations for bayesian variable selection, *Neural Networks* 61 (2015) 22–31.
- [11] X. Cheng, N. S. Chatterji, P. L. Bartlett, M. I. Jordan, Underdamped langevin mcmc: A non-asymptotic analysis, in: *Conference on learning theory*, PMLR, 2018, pp. 300–323.

- [12] J. Song, S. Zhao, S. Ermon, A-nice-mc: Adversarial training for mcmc, *Advances in Neural Information Processing Systems* 30 (2017).
- [13] D. Levy, M. D. Hoffman, J. Sohl-Dickstein, Generalizing hamiltonian monte carlo with neural networks, *arXiv preprint arXiv:1711.09268* (2017).
- [14] L. Galliano, R. Rende, D. Coslovich, Policy-guided monte carlo on general state spaces: Application to glass-forming mixtures, *The Journal of Chemical Physics* 161 (2024).
- [15] S. Liu, S. Sun, Adversarially training mcmc with non-volume-preserving flows, *Entropy* 24 (2022) 415.
- [16] S. Asghar, Q.-X. Pei, G. Volpe, R. Ni, Efficient rare event sampling with unsupervised normalising flows, *arXiv preprint arXiv:2401.01072* (2024).
- [17] S.-H. Li, L. Wang, Neural network renormalization group, *Physical review letters* 121 (2018) 260601.
- [18] F. Noé, S. Olsson, J. Köhler, H. Wu, Boltzmann generators: Sampling equilibrium states of many-body systems with deep learning, *Science* 365 (2019) eaaw1147.
- [19] J. Köhler, L. Klein, F. Noé, Equivariant flows: exact likelihood generative learning for symmetric densities, in: *International conference on machine learning*, PMLR, 2020, pp. 5361–5370.
- [20] D. Boyda, G. Kanwar, S. Racanière, D. J. Rezende, M. S. Albergo, K. Cranmer, D. C. Hackett, P. E. Shanahan, Sampling using su (n) gauge equivariant flows, *Physical Review D* 103 (2021) 074504.
- [21] L. Vaitl, K. A. Nicoli, S. Nakajima, P. Kessel, Gradients should stay on path: better estimators of the reverse-and forward kl divergence for normalizing flows, *Machine Learning: Science and Technology* 3 (2022) 045006.
- [22] M. S. Albergo, D. Boyda, K. Cranmer, D. C. Hackett, G. Kanwar, S. Racanière, D. J. Rezende, F. Romero-López, P. E. Shanahan, J. M. Urban, Flow-based sampling in the lattice schwinger model at criticality, *Physical Review D* 106 (2022) 014514.

- [23] M. Gerdes, P. de Haan, C. Rainone, R. Bondesan, M. C. Cheng, Learning lattice quantum field theories with equivariant continuous flows, arXiv preprint arXiv:2207.00283 (2022).
- [24] L. Felardos, Data-free Generation of Molecular Configurations with Normalizing Flows, Ph.D. thesis, Université Grenoble Alpes, 2022.
- [25] S. van Leeuwen, A. P. d. A. Ortíz, M. Dijkstra, A boltzmann generator for the isobaric-isothermal ensemble, arXiv preprint arXiv:2305.08483 (2023).
- [26] M. Plainer, H. Stark, C. Bunne, S. Günnemann, Transition path sampling with boltzmann generator-based mcmc moves, in: NeurIPS 2023 AI for Science Workshop, 2023.
- [27] Q. Liu, D. Wang, Stein variational gradient descent: A general purpose bayesian inference algorithm, Advances in neural information processing systems 29 (2016).
- [28] Q. Liu, Stein variational gradient descent as gradient flow, Advances in neural information processing systems 30 (2017).
- [29] T. Salimans, D. Kingma, M. Welling, Markov chain monte carlo and variational inference: Bridging the gap, in: International conference on machine learning, PMLR, 2015, pp. 1218–1226.
- [30] Y. Zhang, J. M. Hernández-Lobato, Ergodic inference: Accelerate convergence by optimisation, arXiv preprint arXiv:1805.10377 (2018).
- [31] R. Habib, D. Barber, Auxiliary variational mcmc, in: International Conference on Learning Representations, 2018.
- [32] F. Ruiz, M. Titsias, A contrastive divergence for combining variational inference and mcmc, in: International Conference on Machine Learning, PMLR, 2019, pp. 5537–5545.
- [33] H. Wu, J. Köhler, F. Noé, Stochastic normalizing flows, Advances in Neural Information Processing Systems 33 (2020) 5933–5944.
- [34] Z. Shen, M. Heinonen, S. Kaski, De-randomizing mcmc dynamics with the diffusion stein operator, Advances in Neural Information Processing Systems 34 (2021) 17507–17517.

- [35] J. Sohl-Dickstein, E. Weiss, N. Maheswaranathan, S. Ganguli, Deep unsupervised learning using nonequilibrium thermodynamics, in: International conference on machine learning, PMLR, 2015, pp. 2256–2265.
- [36] J. Ho, A. Jain, P. Abbeel, Denoising diffusion probabilistic models, *Advances in neural information processing systems* 33 (2020) 6840–6851.
- [37] Y. Song, J. Sohl-Dickstein, D. P. Kingma, A. Kumar, S. Ermon, B. Poole, Score-based generative modeling through stochastic differential equations, *arXiv preprint arXiv:2011.13456* (2020).
- [38] Y. Song, C. Durkan, I. Murray, S. Ermon, Maximum likelihood training of score-based diffusion models, *Advances in Neural Information Processing Systems* 34 (2021) 1415–1428.
- [39] Q. Zhang, Y. Chen, Path integral sampler: a stochastic control approach for sampling, *arXiv preprint arXiv:2111.15141* (2021).
- [40] J. Berner, L. Richter, K. Ullrich, An optimal control perspective on diffusion-based generative modeling, *arXiv preprint arXiv:2211.01364* (2022).
- [41] F. Vargas, W. Grathwohl, A. Doucet, Denoising diffusion samplers, *arXiv preprint arXiv:2302.13834* (2023).
- [42] L. Richter, J. Berner, G.-H. Liu, Improved sampling via learned diffusions, *arXiv preprint arXiv:2307.01198* (2023).
- [43] B. Máté, F. Fleuret, Learning interpolations between boltzmann densities, *Transactions on Machine Learning Research* (2023).
- [44] D. P. Kingma, M. Welling, et al., An introduction to variational autoencoders, *Foundations and Trends® in Machine Learning* 12 (2019) 307–392.
- [45] B. D. Anderson, Reverse-time diffusion equation models, *Stochastic Processes and their Applications* 12 (1982) 313–326.
- [46] R. Rombach, A. Blattmann, D. Lorenz, P. Esser, B. Ommer, High-resolution image synthesis with latent diffusion models, in: *Proceedings of the IEEE/CVF conference on computer vision and pattern recognition*, 2022, pp. 10684–10695.

- [47] C. Fu, K. Yan, L. Wang, W. Y. Au, M. C. McThrow, T. Komikado, K. Maruhashi, K. Uchino, X. Qian, S. Ji, A latent diffusion model for protein structure generation, in: Learning on Graphs Conference, PMLR, 2024, pp. 29–1.
- [48] B. Zheng, G. Sun, L. Dong, S. Wang, Ld-csnet: A latent diffusion-based architecture for perceptual compressed sensing, Neural Networks (2024) 106541.
- [49] K. Choi, C. Meng, Y. Song, S. Ermon, Density ratio estimation via infinitesimal classification, in: International Conference on Artificial Intelligence and Statistics, PMLR, 2022, pp. 2552–2573.
- [50] R. T. Chen, Y. Rubanova, J. Bettencourt, D. K. Duvenaud, Neural ordinary differential equations, Advances in neural information processing systems 31 (2018).
- [51] L. Dinh, J. Sohl-Dickstein, S. Bengio, Density estimation using real nvp, arXiv preprint arXiv:1605.08803 (2016).
- [52] D. Dua, C. Graff, Uci machine learning repository, <https://archive.ics.uci.edu/ml/index.php>, 2017. Accessed: 2022-03-13.
- [53] Y. Zhang, Z. Ghahramani, A. J. Storkey, C. Sutton, Continuous relaxations for discrete hamiltonian monte carlo, Advances in Neural Information Processing Systems 25 (2012).
- [54] S. Zheng, J. He, C. Liu, Y. Shi, Z. Lu, W. Feng, F. Ju, J. Wang, J. Zhu, Y. Min, et al., Towards predicting equilibrium distributions for molecular systems with deep learning, arXiv preprint arXiv:2306.05445 (2023).
- [55] B. Jing, E. Erives, P. Pao-Huang, G. Corso, B. Berger, T. Jaakkola, Eigenfold: Generative protein structure prediction with diffusion models, arXiv preprint arXiv:2304.02198 (2023).
- [56] A. Gretton, K. M. Borgwardt, M. J. Rasch, B. Schölkopf, A. Smola, A kernel two-sample test, The Journal of Machine Learning Research 13 (2012) 723–773.